INORGANIC CHEMISTRY FRONTIERS

RESEARCH ARTICLE

View Article Online
View Journal | View Issue

Cite this: *Inorg. Chem. Front.*, 2024, **11**, 7142

Interface engineering of Co_2B–MoO_3/MOF heterojunctions with rich cobalt defects for highly enhanced $NaBH_4$ hydrolysis†

Chenxi Shang,[a] Luyan Shi,[a] Shuqing Zhou,[a] Sheraz Muhammad,[a] Tayirjan Taylor Isimjan,*[b] Huancheng Hu *[a] and Xiulin Yang *[a]

Received 9th July 2024,
Accepted 4th September 2024

DOI: 10.1039/d4qi01721h

rsc.li/frontiers-inorganic

Sodium borohydride (SBH) is a promising hydrogen storage material, but efficient catalysts for H_2 generation from its hydrolysis are needed for practical use. In this work, a self-sacrificial template strategy was employed to synthesize Co_2B–MoO_3/MOF heterojunction materials with rich cobalt defects on MOF substrates. The optimal Co_2B–MoO_3/MOF catalyst exhibited a rapid hydrogen generation rate of 6893.1 mL min^{-1} g_{cat}^{-1} at 25 °C, outperforming most non-precious metal catalysts. Studies found that the higher work function (6.94 eV) and charge attraction properties (–15.75 mV) endow the Co_2B-MoO_3/MOF catalyst with a strong adsorption capacity for negatively charged BH_4^-. Based on the Michaelis–Menten model, a Co_2B–MoO_3/MOF-catalyzed mechanism for the hydrolysis of $NaBH_4$ to generate H_2 was proposed, in which Co_2B and MoO_3 effectively activate the BH_4^- and H_2O molecules, respectively. Moreover, a highly selective "on–off" switch was achieved *via* a Zn^{2+}/EDTA-2Na system for on-demand H_2 evolution upon $NaBH_4$ hydrolysis. Hydrogen generated from $NaBH_4$ hydrolysis by the Co_2B–MoO_3/MOF catalyst was used directly to drive a custom H_2–air fuel cell, successfully powering an electric fan and demonstrating its potential for practical applications.

Introduction

Hydrogen is a high-energy-density, clean energy source with significant potential to replace fossil fuels.[1,2] One of its critical applications is as a fuel in hydrogen–oxygen fuel cells, which can power devices, including portable electronics, spacecrafts, and vehicles.[3] Typically, hydrogen is stored and transported as a high-pressure gas or liquefied gas, which poses safety concerns and incurs high costs.[4] Sodium borohydride ($NaBH_4$) is a safe and efficient chemical hydrogen storage material that can release high-purity hydrogen through hydrolysis or methanol decomposition under mild conditions, providing an economical and environmentally friendly solution for hydrogen storage and transportation.[5] Hydrogen production from sodium borohydride is highly versatile, serving as an efficient hydrogen source for the clean energy sector while also playing a crucial role in healthcare and organic chemical synthesis.[6] Of particular note, the byproduct of $NaBH_4$ hydrolysis, sodium metaborate ($NaBO_2$), is non-toxic and can be recycled to regenerate $NaBH_4$. This cyclic mechanism enables the $NaBH_4$–H_2–PEMFC system to flexibly provide power on demand, making it a significant power supply device.[7] However, $NaBH_4$ typically exhibits slow self-hydrolysis ($NaBH_4 + 2H_2O \rightarrow NaBO_2 + 4H_2$) under ambient conditions.[8] Therefore, it is desirable to develop highly efficient catalysts to accelerate the reaction rate.

To date, noble metals such as Pt,[9] Pd,[10] Ru,[11] and Rh[12] have proven exceptionally efficient for the hydrolysis of $NaBH_4$, with high hydrogen generation rates. However, the high cost and limited availability of these metals have hindered the widespread application of noble metal nanoparticles.[13] Recently, transition metal borides have attracted attention due to their electronic effects and environmental friendliness; in particular, the M to B electron transfer process effectively promotes the desorption of H_2 from the metal boride surface.[14] Yet, transition metal borides are less stable for the hydrolysis of $NaBH_4$, with most rapidly losing activity over cycles due to the agglomeration of nanoparticles over time because of their high surface energy. Therefore, it is necessary to confine or immobilize transition metal nano-catalysts in a support material (MOFs, carbon, graphene, *etc.*) to enhance their activity and stability in heterogeneous catalysis.[15,16] In view of

[a]*Guangxi Key Laboratory of Low Carbon Energy Materials, School of Chemistry and Pharmaceutical Sciences, Guangxi Normal University, Guilin 541004, China. E-mail: xlyang@gxnu.edu.cn, siniantongnian@126.com*
[b]*Saudi Arabia Basic Industries Corporation (SABIC) at King Abdullah University of Science and Technology (KAUST), Thuwal 23955-6900, Saudi Arabia. E-mail: isimjant@sabic.com*

† Electronic supplementary information (ESI) available. See DOI: https://doi.org/10.1039/d4qi01721h

this, Tsumori *et al.*[17] used the impregnation method to introduce Au nanoparticles into Cr-MIL-101, and then thermally induced de-ligand degradation to form quasi-MIL-101 with accessible Cr–O sites for low-temperature CO oxidation. The method retains the MOF framework structure and functional groups while producing highly active and stable metals/metal oxides. Furthermore, defect engineering is recognized as an effective strategy for regulating surface charge distribution and optimizing active sites.[18] For instance, Zhou *et al.* introduced cobalt defects into Ru/Co–Sm_2O_3, optimizing intermediate adsorption.[19] Wang *et al.* enhanced ion transfer and improved the electronic structure by forming cobalt defects in CoS_2 through co-doping.[20] In our previous work, we confirmed the feasibility of this defect engineering approach by creating highly efficient $NaBH_4$ hydrolysis catalysts rich in phosphorus and oxygen vacancies.[21,22]

Efforts to enhance the hydrolysis activity of sodium borohydride have focused on various strategies, including the construction of optimized structures and heterojunctions. Creating intimate heterojunctions not only forms a hierarchical pore framework with more exposed surfaces, facilitating shorter paths for accelerated ionic diffusion, but also generates abundant crystalline/amorphous heterointerfaces with modified electronic structures for rapid electron transfer.[23] For example, Kavinkumar *et al.* observed binding energy shifts in the $NiCo_2O_4/MoO_2$@ALD–NiO heterostructure, signifying charge redistribution and electron transfer, modulating the hetero-nanostructure's electronic properties.[24] Overall, in heterogeneous structures, the hybridization of different components enhances the catalyst's performance compared to a single-component catalyst by improving absorption/desorption capabilities, electronic regulation, atomic arrangement, and interface stability.[25] MoO_3 has become a popular target in this field due to its low toxicity, high theoretical capacity (1117 mA h g^{-1}), capability for multiple electron transfers, and large work function.[26,27] Despite its typical chemical inertness in alkaline solutions at room temperature, when mixed with cobalt (Co) catalysts, it acts as a facilitator, promoting the formation of highly active heterostructures.[28] According to the Brewer–Engel valence bond theory, combining a Co atom with two paired d electron orbitals and a Mo atom with five half-filled d electron orbitals can result in a synergistic effect within the compound.[29] Bimetallic synergism optimizes structural and electronic properties, offering new opportunities for developing catalysts with dual transition metal heterostructures.[30]

Herein, we propose a self-sacrificial template strategy coupled with a smart "*in situ* seeding" process for synthesizing Co_2B–MoO_3/MOF heterojunction materials with rich cobalt defects on MOF substrates. Experimental and characterization analyses showed that introducing cobalt defects optimized the electronic structure of the materials, facilitating the rapid transfer of ions. The hydrophilic porous nanostructures provide efficient pathways for mass/charge transfer of reactants and create abundant active sites. Particularly noteworthy is the synergistic effect of the Co_2B and MoO_3 components, which effectively activated the BH_4^- and H_2O molecules to promote hydrolysis. Furthermore, controllable on-demand hydrogen generation was achieved by introducing unique chemical switches for the "on–off" hydrolysis of $NaBH_4$. This study may provide a better understanding of the cooperative roles of different active sites on the heterostructured catalyst and the reaction mechanism conducive to the rational design of inexpensive and robust catalysts for the hydrolysis of $NaBH_4$ for hydrogen generation.

Results and discussion

The Co_2B–MoO_3/MOF heterojunction materials were synthesized through a series of steps, including room temperature wet dipping and chemical reduction methods, as depicted in Fig. 1a. Initially, Co-BTC bulk microspheres were prepared using a solvothermal method. The X-ray diffraction (XRD) pattern in Fig. S1a† and the Fourier transform infrared (FTIR) spectra in Fig. S1b† show a structure similar to that previously reported for Co-BTC.[31] Subsequently, after dispersing the MOF in ethanol *via* ultrasound, the Co^{2+}/Mo^{6+}-MOF was prepared by adding $CoCl_2{\cdot}6H_2O$ and $Na_2MoO_4{\cdot}2H_2O$, followed by stirring and vacuum evaporation. Finally, the Co^{2+}/Mo^{6+}-MOF and urea were added to a mortar for grinding, followed by chemical reduction etching to obtain Co_2B–MoO_3/MOF heterojunction materials with abundant cobalt defects. As shown in Fig. 1b, the $NaBH_4$ reduction treatment led to the destruction of the MOF scaffold and the coexistence of Co_2B (JCPDS: 25-0241) and MoO_3 phases (JCPDS: 21-0569) was detected, indicating the successful construction of Co_2B–MoO_3/MOF heterojunction materials. The control samples were also characterized using XRD. Fig. S2a† confirms that the Co_2B–Co/MOF comprises Co_2B and a small amount of cobalt. Fig. S2b† confirms that the MoB/MOF is predominantly composed of MoB. The N_2 absorption/desorption isotherm of the Co_2B–MoO_3/MOF is shown in Fig. S3a,† which features IV isothermal curves, and the curves of adsorption and desorption processes do not coincide, forming an H3 hysteresis loop, indicating the presence of mesopores.[32] The BET specific surface area of the Co_2B–MoO_3/MOF was 18.3 m^2 g^{-1}, and the average pore size was 32.9 nm, as shown in Fig. S3a and b.† This porous heterostructure can accommodate more surface-active sites, greatly facilitate charge carriers' diffusion/drift processes, and provide efficient transport pathways for reactants and products, enhancing sodium borohydride hydrolysis.[33] Electron paramagnetic resonance (EPR) is an excellent and efficient tool for identifying the concentration and existence of defects. Fig. 1c shows a signal at g = 2.12, indicating the successful introduction of cobalt defects. This may result from the partial reduction or recombination of some cobalt ions in the complex formed by cobalt chloride and urea during sodium borohydride reduction.[34] Compared with Co_2B and the Co_2B–Co/MOF, the Co_2B–MoO_3/MOF exhibits much stronger signals, which may be due to the doping of Mo^{6+}, causing a redistribution of charge and leading to the formation of more cobalt defects to

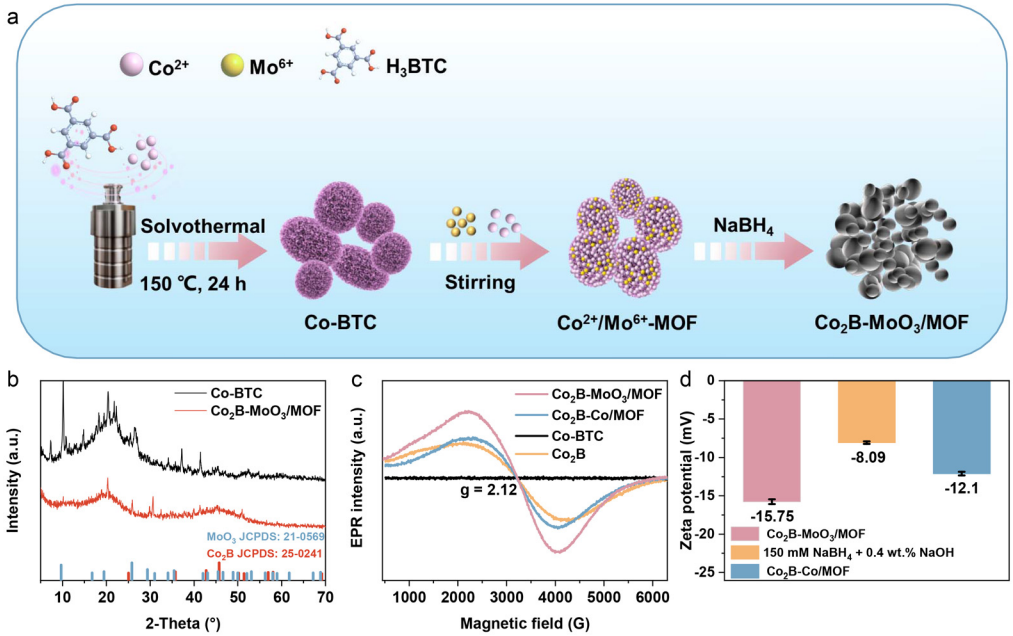

Fig. 1 (a) Schematic illustration of the preparation of the Co_2B–MoO_3/MOF. (b) XRD patterns of the Co_2B–MoO_3/MOF and Co-BTC. (c) EPR spectra of the Co_2B–MoO_3/MOF, the Co_2B–Co/MOF, Co_2B, and Co-BTC. (d) Zeta potentials of the Co_2B–MoO_3/MOF, 150 mM $NaBH_4$ + 0.4 wt% NaOH solution, and the Co_2B–Co/MOF.

balance the additional charge introduced by doping.[35] In summary, the formation of abundant cobalt defects in the Co_2B–MoO_3/MOF can change the carrier concentration of the catalyst and enhances the synergistic effect between the components, resulting in better catalytic performance.[36] Given the challenges associated with directly measuring catalyst surface potentials through experimental methods, zeta potential (ζ) measurements have become a widely adopted alternative method for assessing the surface charge properties of materials. As shown in Fig. 1d, the zeta potential of 150 mM $NaBH_4$ + 0.4 wt% NaOH solution was −8.09 mV. Comparatively, the zeta potential of the Co_2B–MoO_3/MOF is much lower than those of the Co_2B–Co/MOF and 150 mM $NaBH_4$ + 0.4 wt% NaOH solution, indicating that the Co_2B–MoO_3/MOF heterojunction material has a strong adsorption capacity for negatively charged BH_4^-, which is a critical factor for the superior hydrolysis performance exhibited in the sodium borohydride ($NaBH_4$) hydrolysis reaction.[37]

Scanning electron microscopy (SEM) and transmission electron microscopy (TEM) were performed to study the microstructures of the Co_2B–MoO_3/MOF. Co-BTC exhibits a blocky microsphere structure (Fig. S4a†). In Fig. 2a, the Co_2B–MoO_3/MOF displays regular nano-aggregates. The self-assembled nano-aggregates form a three-dimensional nano-forest structure, and numerous micro/nanopores can be observed. This observation suggests that porous nanostructures promote mass/charge transfer and active site exposure during hydrolysis reactions.[38] In Fig. S4b,† the Co_2B–Co/MOF also displays regular nano-aggregates. In contrast, the Co_2B catalyst prepared without the MOF template showed irregular particle agglomeration (Fig. S4c†), indicating that the self-sacrificial template strategy effectively constructs nanoparticles' structural components and inhibits aggregation. Obvious grain boundaries were observed in the TEM image (Fig. 2b) of the Co_2B–MoO_3/MOF, showing that it was composed of nanoparticles, which is in good agreement with the SEM results. Furthermore, a clear boundary between Co_2B and MoO_3 was observed (Fig. 2c), and the HR-TEM image clearly shows lattice fringes with interplanar distances of 0.21 nm and 0.28 nm, which match well with the (211) and (204) planes of Co_2B and MoO_3, respectively. This indicates that the constructed heterojunction has many tight interfaces, facilitating the movement of electrons across the interface.[39] The TEM image also shows that the Co_2B–Co/MOF material is an aggregate composed of nanoclusters (Fig. S5†). The corresponding elemental mappings of the Co_2B–MoO_3/MOF demonstrate the homogeneous distribution of Co, Mo, B, and O elements (Fig. 2d). Overall, constructing a heterostructure can generate a synergistic effect and overcome the limitations of a single component, leading to improved hydrolysis performance of sodium borohydride. Contact angle (CA) experiments were conducted to test the hydrophilicity of the catalyst. The Co_2B–MoO_3/MOF exhibits a cambered water droplet with a contact angle of 22.97°, significantly lower than those of the Co_2B–Co/MOF (40.79°) and Co_2B (37.96°), demonstrating its superior hydrophilicity (Fig. 2e). This phenomenon reflects the strong adsorption of interfacial water on the catalyst surface, due to the high hydrophilicity of the Mo species doped with Mo–O coordination.[40]

The formation of heterojunctions can lead to the redistribution of electrons at the interface, enhancing the activity of

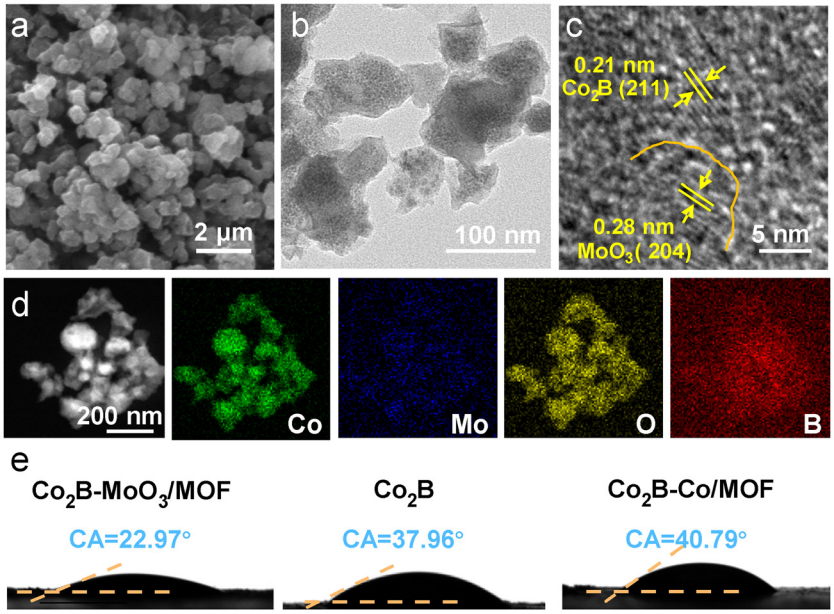

Fig. 2 (a) SEM image of the $Co_2B–MoO_3$/MOF. (b) TEM and (c) high-resolution TEM (HR-TEM) images of the $Co_2B–MoO_3$/MOF. (d) HAADF-STEM image and the corresponding elemental mappings (Co, Mo, B, and O) of the $Co_2B–MoO_3$/MOF. (e) Contact angle measurement of different catalysts.

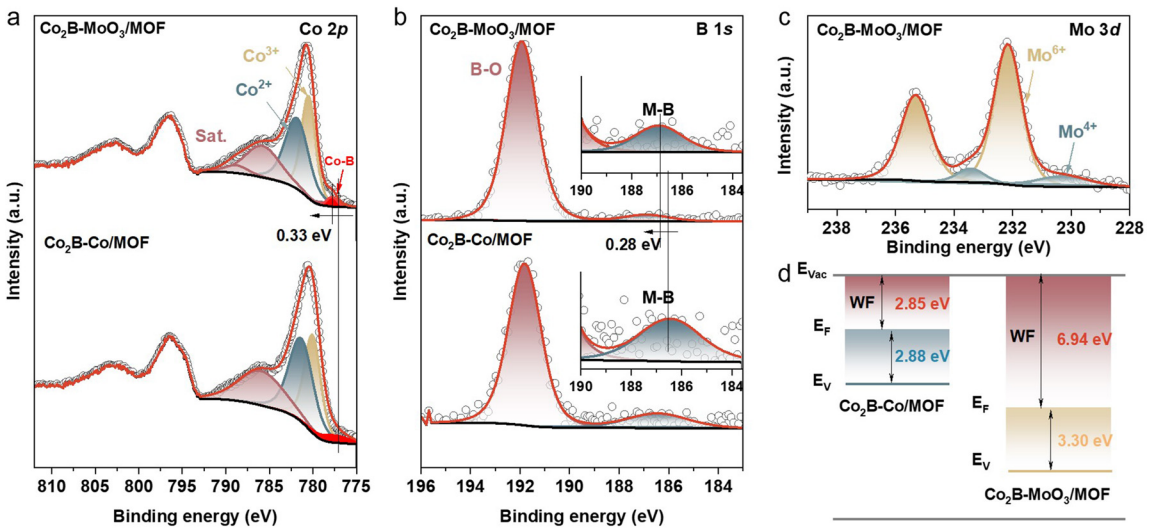

Fig. 3 High-resolution XPS spectra of (a) Co 2p and (b) B 1s for the $Co_2B–MoO_3$/MOF and $Co_2B–Co$/MOF and of (c) Mo 3d for the $Co_2B–MoO_3$/MOF. (d) Band structure alignment of the $Co_2B–Co$/MOF and $Co_2B–MoO_3$/MOF.

active sites. X-ray photoelectron spectroscopy (XPS) was utilized to study the surface electronic states and composition of the $Co_2B–MoO_3$/MOF and $Co_2B–Co$/MOF. The survey spectra confirm the presence of Co, Mo, B, and O elemental dispersion in the prepared $Co_2B–MoO_3$/MOF (Fig. S6†). The Na 1s peak (1072.2 eV) appears in the full spectrum, possibly due to Na ions as impurities dissolved in the solution during the dehydrogenation of SBH.[41] High-resolution XPS spectra of the C 1s regions were analyzed using C–C (284.8 eV), C–O (286.0 eV), and C═O (288.7 eV) as calibration criteria (Fig. S7a and b†).[42] For Co 2p (Fig. 3a), the peaks located at 777.8/777.4 eV, 780.5/780.1 eV, 781.8/781.4 eV, and 785.8/785.9 eV correspond to Co^0/Co–B, Co^{3+}, Co^{2+} and the satellite, respectively. The B 1s core-level XPS spectra of the $Co_2B–MoO_3$/MOF and $Co_2B–Co$/MOF were deconvoluted into two peaks representing metal–B/B^0 and B–O bonds, revealing the presence of a metal–B alloy (Fig. 3b).[43] Moreover, compared with the $Co_2B–Co$/MOF, the binding energies of the Co–B and M–B peaks of the $Co_2B–MoO_3$/MOF are positively shifted by 0.33 eV and 0.28 eV. This result indicates a change in the local electron density of Co in

Co_2B–MoO_3/MOF heterojunction materials, with the Co sites likely acting as electron donors.[44] The binding energies of Co–B and M–B species increase after Mo doping, with the peak shift towards higher binding energies also signifying the downshift of the d-band center referenced to the Fermi level. Considering that the d-band structure is directly related to the adsorption ability of H* on the catalyst surface, favorable tuning of hydrogen generation reaction (HGR) activity is expected in the Co_2B–MoO_3/MOF.[45] As for the Mo 3d signal, the peaks detected at 232.1/235.3 eV are attributed to Mo^{6+}, while the peaks centered at 230.1/233.4 eV are assigned to Mo^{4+} (Fig. 3c). The Mo dopant in the Co_2B–MoO_3/MOF catalysts mainly exists in the form of MoO_2/MoO_3.[46] The XPS spectrum of O 1s in Fig. S7c† shows peaks at 530.3, 531.4, and 532.3 eV assigned to oxygen–metal (O–M), carbon–oxygen (C–O), and surface chemisorption water (H_2O), respectively. Furthermore, ultraviolet photoelectron spectroscopy (UPS) was used to determine the bandgap position of the target Co_2B–MoO_3/MOF by measuring the work function and the valence band maximum with respect to the Fermi level (Fig. S8a†). The potential depends on the work function; a larger work function results in a more positive potential ϕ (e^-), indicating a stronger oxidation ability and the ability to accept electrons into the material.[47] The work function (WF) of the Co_2B–MoO_3/MOF, at 6.94 eV, is significantly higher than that of the Co_2B–Co/MOF at 2.85 eV (Fig. S8b†), meaning that BH_4^- is more easily adsorbed on the surface of Co_2B–MoO_3/MOF catalysts. The valence band maximum values were determined to be approximately 3.30 eV for the Co_2B–MoO_3/MOF and 2.88 eV for the Co_2B–Co/MOF, respectively (Fig. 3d). Clearly, the valence band shifts toward the Fermi level after Mo doping of the catalyst.[48] The XPS and UPS characterization results confirm that the Co_2B–MoO_3/MOF heterostructure effectively regulates active sites and promotes rapid electron transfer, enhancing sodium borohydride's hydrolysis performance.

The properties of the catalysts were evaluated in a 150 mM $NaBH_4$ (with 0.4 wt% NaOH) solution at 25 °C, with the reaction setup schematically depicted in Fig. S9.† In the absence of a catalyst, faint autohydrolysis was observed in the 150 mM $NaBH_4$ aqueous solution (Fig. S10a†), and almost no autohydrolysis was observed in the 150 mM $NaBH_4$ aqueous solution with 0.4 wt% NaOH (Fig. S10b†). Initially, the improvement of the hydrolysis properties of sodium borohydride by different catalyst types was investigated. Through the study of the Co_2B–MoO_3/MOF, the Co_2B–Co/MOF, the MoB/MOF, and Co_2B, it was found that the Co_2B–MoO_3/MOF catalyst exhibited the fastest hydrolysis kinetics, significantly surpassing the other catalysts, with a hydrogen generation rate of 6893.1 mL min^{-1} g^{-1} (Fig. 4a and b). Incorporating a small amount of Mo into the Co_2B–MoO_3/MOF supports Co's surface-active sites and enhances Co's catalytic reactivity, compared to the Co_2B–Co/MOF. This finding confirms the unique electronic structure and surface-active sites between Co_2B and MoO_3 in the Co_2B–MoO_3/MOF.[49] Additionally, the atomic ratio of Co to Mo was found to be about 14 : 1 by ICP-MS (Table S1†), essentially the same as the feeding ratio in the synthesis. Next, the hydrolysis performance of the catalysts for $NaBH_4$ was optimized by varying the Co/Mo molar ratio on the same MOF carrier. As

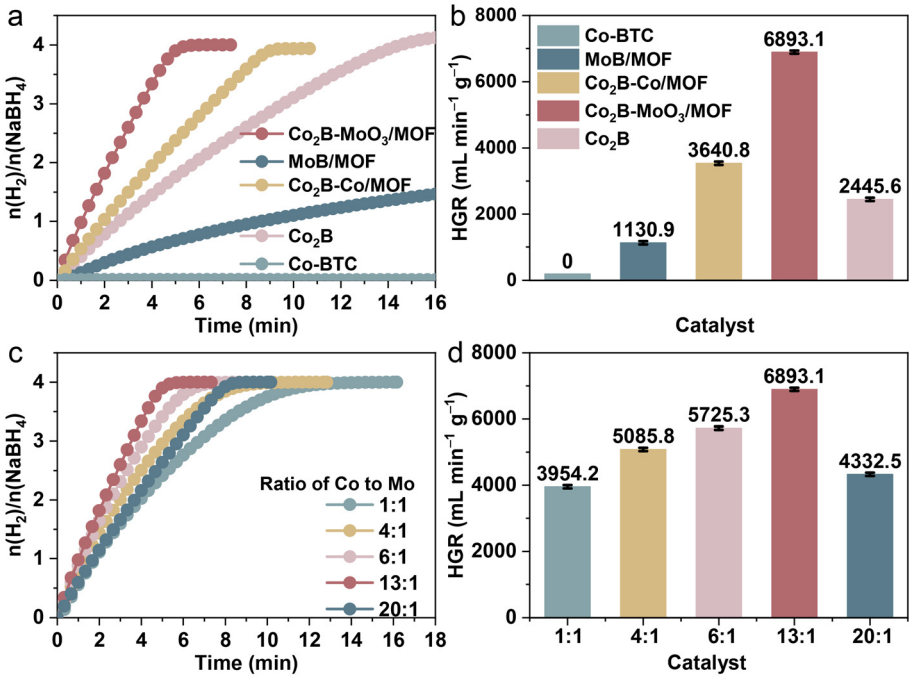

Fig. 4 (a) The equivalent H_2 per mole of sodium borohydride *versus* time with different catalysts and (b) the corresponding HGR values. (c) Stoichiometric H_2 evolution in 150 mM $NaBH_4$ + 0.4 wt% NaOH solution using Co_2B–MoO_3/MOF catalysts with different ratios of Co to Mo at 25 °C and (d) the corresponding HGR values.

shown in Fig. 4c and d, the H_2 generation rate increased until the molar ratio reached 13/1 and then decreased as the Co content continued to increase. This suggests that a high Co/Mo molar ratio may affect the electron enrichment between Co_2B and MoO_3.[50]

NaOH is usually introduced as a stabilizer into the $NaBH_4$ hydrolysis system to prevent self-hydrolysis. Fig. 5a shows that the H_2 generation rate barely changed as the NaOH concentration increased from 0 wt% to 0.8 wt%, indicating that sodium borohydride is stable under alkaline conditions, consistent with previous studies.[19] Based on the principles of green chemistry, 0.4 wt% sodium hydroxide was chosen as the stabilizing agent for hydrolysis. To explore the effect of $NaBH_4$ concentration on catalytic H_2 production, we kept the NaOH concentration constant at different $NaBH_4$ concentrations. Fig. 5b shows that varying the amount of sodium borohydride did not significantly change the hydrogen generation rate. The relationship between ln(rate) and ln(concentration of $NaBH_4$) is depicted in the inset of Fig. 5b, and the slope value obtained corresponds to 0.060, which is close to zero. These results suggest that the hydrolysis reaction of $NaBH_4$ is a zero-order reaction independent of the concentration of $NaBH_4$.[51] To evaluate the effect of catalyst dosage on the hydrolysis of $NaBH_4$, the reaction was carried out using catalysts weighing 5, 10, 15, and 20 mg while maintaining other parameters constant. Fig. S11a and b† show that 10 mg of the Co_2B–MoO_3/MOF catalyst exhibits the highest hydrogen generation rate, making it the optimal amount of the catalyst and resulting in substantial cost reduction.

The reaction was conducted at various temperatures (25, 30, 35, 40, and 45 °C) while keeping the concentrations of the Co_2B–MoO_3/MOF catalyst and sodium borohydride alkali solution constant to obtain the activation energy (E_a). As shown in Fig. 5c and Fig. S12,† the hydrogen generation rate increases significantly with rising temperature and exhibits a nearly linear relationship with the reaction time. According to the Arrhenius plot, the calculated E_a values of the Co_2B–MoO_3/MOF and Co_2B–Co/MOF were 50.50 and 51.57 kJ mol^{-1}, respectively (Fig. 5d). However, the hydrogen production efficiency depends on multiple factors, including catalyst activity, component synergy, and reaction conditions, which may challenge direct comparisons based solely on the activation energy.

The reusability of the Co_2B–MoO_3/MOF was evaluated due to its significance for practical applications (Fig. 5e and f). The results indicate that while the catalytic activity declines with increasing cycles, the decrease is less pronounced compared to the Co_2B–Co/MOF (Fig. S13a and b†), demonstrating better reusability. To determine the exact reasons for the slight decrease in catalytic activity, the Co_2B–MoO_3/MOF after five cycles was characterized with XRD, SEM, XPS and ICP. As demonstrated in Fig. S14,† the XRD pattern shows that the Co_2B–MoO_3/MOF, after five cycles, has a similar structural composition. The SEM images reveal surface agglomeration of the catalysts after catalyzing the hydrolysis of $NaBH_4$ (Fig. S15†). Additionally, XPS analysis of the stabilized sample revealed the presence of Co, Mo, and B elements in the full spectrum, consistent with the results prior to the cyclic reaction (Fig. S16†). Moreover, XPS analysis (Fig. S17a–c†) shows that the original elemental composition, chemical state, and peak intensities were similar to those of the Co_2B–MoO_3/MOF even after five cycles. ICP analyses further confirmed the stabi-

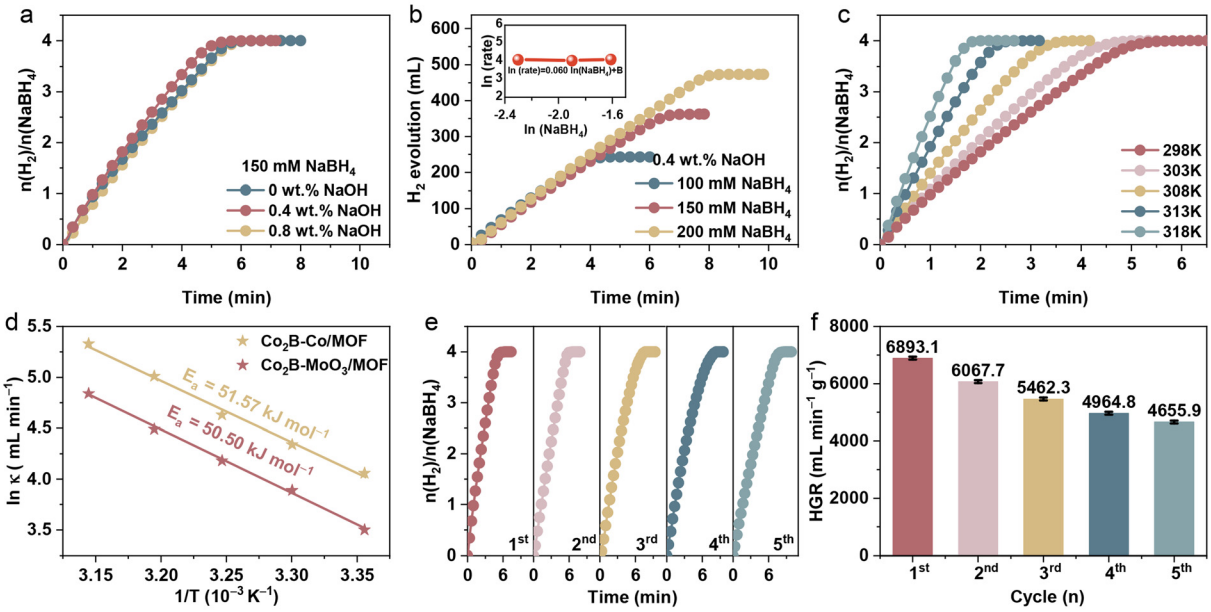

Fig. 5 (a) Effect of different NaOH contents on the HGR of the Co_2B–MoO_3/MOF at the same $NaBH_4$ concentration (150 mM). (b) Effect of different $NaBH_4$ contents on the HGR of the Co_2B–MoO_3/MOF at a fixed NaOH concentration (0.4 wt%). (c) Curves of the hydrolysis of alkaline $NaBH_4$ solution at different reaction temperatures in the range of 298–318 K. (d) Arrhenius plots of the Co_2B–MoO_3/MOF and Co_2B–Co/MOF. (e) Reusability test of the Co_2B–MoO_3/MOF catalyst in alkaline $NaBH_4$ solution at 25 °C and (f) the corresponding HGR values in the different cycles.

lity of the catalysts, revealing only a minimal reduction in molybdenum content even after five cycles (Table S1†). Therefore, the slight decrease in catalyst performance can be attributed to two main factors: the formation of very low water-soluble $NaBO_2$, which encapsulates the catalyst particles, and a small amount of molybdenum exfoliation.[52]

As discussed above, the designed Co_2B–MoO_3/MOF catalyst exhibits excellent catalytic activity, primarily due to the composition of hybrid materials and the strong interaction between different components. The formation of Co_2B–MoO_3/MOF heterojunctions not only optimizes the electronic structure at the heterointerfaces but also tunes the BH_4^- adsorption and dissociation behavior. As shown in Fig. 6a, a possible reaction mechanism based on the Michaelis–Menten model[53] has been proposed to catalyze the hydrolysis of $NaBH_4$ for H_2 generation. It is well established that transition-metal (hydro) oxides exhibit higher oxophilicity, enabling rapid HO–H bond cleavage.[54] Thus, BH_4^- tends to adsorb at the Co_2B site of the Co_2B–MoO_3/MOF heterostructure, while H_2O adsorbs at the MoO_3 site. The specific steps are as follows: (I) BH_4^- is adsorbed on the surface of Co_2B sites in the Co_2B–MoO_3/MOF catalyst, (II) the B–H bond of BH_4^- dissociates at the Co_2B sites, producing H^- and BH_3 (eqn (1)), (III) the generated H^- on the Co_2B surface quickly interacts with one of the protonic H^+ of H_2O, resulting in the release of one molecule of H_2 (eqn (2)), and the remaining OH^- combines with adsorbed BH_3 to form BH_3OH^- (eqn (3)), (IV) the H in BH_3OH^- generated in the previous step continues to adsorb onto Co_2B, and (V) as the reaction proceeds, the remaining H atoms in the borohydride are replaced by OH^- ions, which are eventually decomposed into $B(OH)_4^-$ species (eqn (4)).[55] These steps illustrate the role of the Co_2B–MoO_3/MOF heterostructure in enhancing the hydrolysis of $NaBH_4$ by efficiently adsorbing and dissociating the reactants, leading to rapid and high-yield hydrogen generation.

$$BH_4^- \rightleftharpoons BH_3 + H^- \quad (1)$$

$$H^- + H_2O \rightleftharpoons H_2 + OH^- \quad (2)$$

$$OH^- + BH_3 \rightleftharpoons BH_3OH^- \quad (3)$$

$$OH^- + BH(OH)_3^- \rightleftharpoons B(OH)_4^- + H^- \quad (4)$$

To effectively and safely produce, transport, and store H_2, there is an urgent need to develop the "on–off" control for on-demand H_2 evolution during $NaBH_4$ hydrolysis. According to previous studies,[56] Zn^{2+} can act as a switching-off agent for hydrogen generation due to its covering effect on the active surface sites, whereas EDTA-2Na can be introduced for subsequent switching on due to its strong coordination ability with Zn^{2+}. Fig. 6b depicts the hydrogen evolution curve of Co_2B–MoO_3/MOF-catalyzed $NaBH_4$ hydrolysis under alternating addition of different chemical switches. The addition of 0.5 M $ZnCl_2$ solution (0.2 mL) significantly inhibited hydrogen release, resulting in the cessation of bubble formation (Fig. 6c). Upon addition of 0.5 M EDTA-2Na solution (0.2 mL), the reaction was reactivated, and hydrogen release resumed.

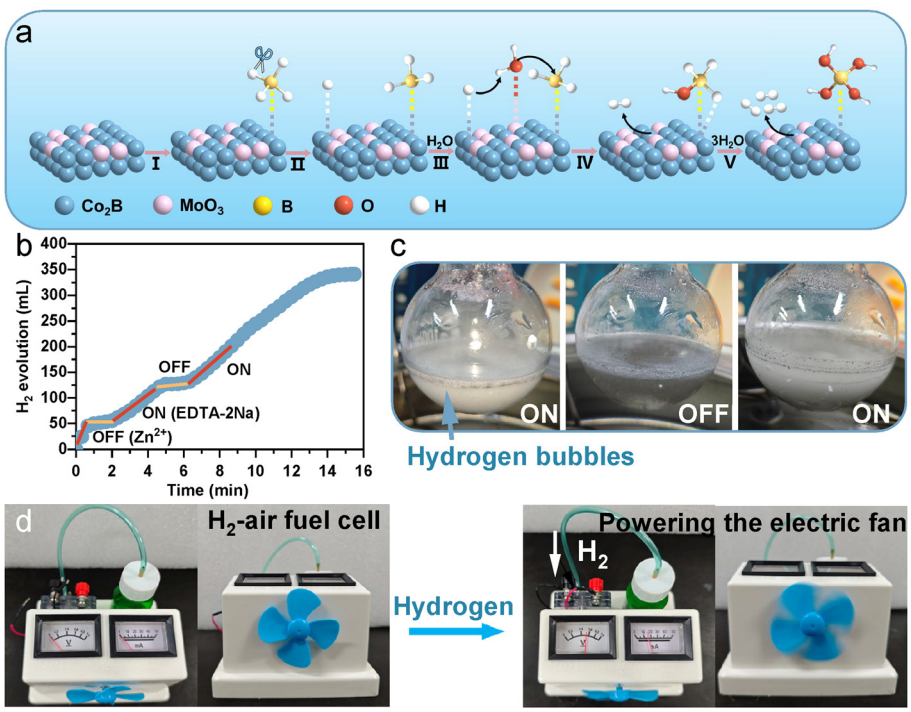

Fig. 6 (a) Proposed mechanism diagram of $NaBH_4$ hydrolysis for H_2 generation. (b) Time plots and (c) photographs of on-demand hydrogen generation over the Co_2B–MoO_3/MOF for $NaBH_4$ hydrolysis with successive addition of $ZnCl_2$ and EDTA-2Na. (d) Photographs of a working electric fan powered by a customized H_2–air fuel cell.

This on–off process using chemical switches can be well reproduced, achieving flexible on-demand hydrogen production. To expand its potential application areas, hydrogen produced by $NaBH_4$ hydrolysis catalyzed by a Co_2B–MoO_3/MOF catalyst was directly supplied to a custom-made H_2–air fuel cell. This fuel cell outputs an operating voltage of about 0.5 V and a current of about 15 mA, successfully driving an electric fan (Fig. 6d). This provides a safer and more reliable method for hydrogen conversion and economically and efficiently converts chemical energy into electricity.

Conclusions

In summary, we report a Co_2B–MoO_3/MOF heterojunction material with rich cobalt defects synthesized on MOF substrates. Analysis indicates that the superior hydrolysis performance of the Co_2B–MoO_3/MOF catalyst is attributed to its hydrophilic porous nanostructures and numerous cobalt defects, and the synergistic electronic interactions among the active species. A reliable catalytic mechanism has been proposed based on various characterization studies and the reaction process. By employing specific chemical switches, the Co_2B–MoO_3/MOF also achieves on-demand hydrogen evolution control. Hydrogen produced by the Co_2B–MoO_3/MOF-catalyzed $NaBH_4$ hydrolysis was successfully used to power a custom-made H_2–air fuel cell, demonstrating the efficient and economical conversion of chemical energy into electrical energy. This provides a safe, economical, and efficient solution for hydrogen utilization and energy conversion in the sustainable energy industry.

Author contributions

Chenxi Shang: investigation, writing – original draft, and data curation. Luyan Shi: investigation. Shuqing Zhou: data curation. Sheraz Muhammad: investigation and methodology. Tayirjan Taylor Isimjan: writing – review and editing. Huancheng Hu: supervision. Xiulin Yang: supervision and writing – review and editing.

Data availability

The data supporting this article have been included as part of the ESI.†

Conflicts of interest

The authors declare that they have no known competing financial interests or personal relationships that could have appeared to influence the work reported in this paper.

Acknowledgements

This work was supported by the National Natural Science Foundation of China (no. 52363028 and 21965005), the Natural Science Foundation of Guangxi Province (2021GXNSFAA076001 and 2018GXNSFAA294077), and the Guangxi Technology Base and Talent Subject (GUIKE AD23023004 and GUIKE AD20297039).

References

1 X. Xu, K. Guo, J. Sun, X. Yu, X. Miao, W. Lu and L. Jiao, Interface engineering of Mo-doped Ni_2P/Fe_xP-V multiheterostructure for efficient dual-pH hydrogen evolution and overall water splitting, *Adv. Funct. Mater.*, 2024, **34**, 2400397.

2 Y. Wu, G. Huang, S. Du, M. Li, Q. Liu, Y. Zhou, Z. Jiang, X. Zhu, Y. Wang, T. Wang, L. Tao and S. Wang, Electrocatalysis boosts the methanol thermocatalytic dehydrogenation for high-purity H_2 and CO production, *J. Am. Chem. Soc.*, 2024, **146**, 9657–9664.

3 J. Liao, Y. Shao, Y. Feng, J. Zhang, C. Song, W. Zeng, J. Tang, H. Dong, Q. Liu and H. Li, Interfacial charge transfer induced dual-active-sites of heterostructured $Cu_{0.8}Ni_{0.2}WO_4$ nanoparticles in ammonia borane methanolysis for fast hydrogen production, *Appl. Catal., B*, 2023, **320**, 121973.

4 M. Xiao, A. Baktash, M. Lyu, G. Zhao, Y. Jin and L. Wang, Unveiling the role of water in heterogeneous photocatalysis of methanol conversion for efficient hydrogen production, *Angew. Chem., Int. Ed.*, 2024, **63**, e202402004.

5 Y. Zhu, L. Ouyang, H. Zhong, J. Liu, H. Wang, H. Shao, Z. Huang and M. Zhu, Closing the loop for hydrogen storage: facile regeneration of $NaBH_4$ from its hydrolytic product, *Angew. Chem., Int. Ed.*, 2020, **59**, 8623–8629.

6 G. Pandey, M. Bhardwaj, S. Kumar, S. D. Lawaniya, M. Kumar, P. K. Dwivedi and K. Awasthi, Synergistic effects of Pd-Ag decoration on SnO/SnO_2 nanosheets for enhanced hydrogen sensing, *Sens. Actuators, B*, 2024, **402**, 135062.

7 L. Shi, K. Zhu, Y. Yang, Q. Liang, Q. Peng, S. Zhou, T. T. Isimjan and X. Yang, Phytic acid-derivative Co_2B-CoPOx coralloidal structure with delicate boron vacancy for enhanced hydrogen generation from sodium borohydride, *Chin. Chem. Lett.*, 2024, **35**, 109222.

8 L. Yao, X. Li, W. Peng, Q. Yao, J. Xia and Z.-H. Lu, Co-CeO_x nanoparticles anchored on a nitrogen-doped carbon nanosheet: a synergistic effect for highly efficient hydrolysis of sodium borohydride, *Inorg. Chem. Front.*, 2021, **8**, 1056–1065.

9 J. Li, X. Hong, Y. Wang, Y. Luo, P. Huang, B. Li, K. Zhang, Y. Zou, L. Sun, F. Xu, F. Rosei, S. P. Verevkin and A. A. Pimerzin, Encapsulated cobalt nanoparticles as a recoverable catalyst for the hydrolysis of sodium borohydride, *Energy Storage Mater.*, 2020, **27**, 187–197.

10 N. Patel, B. Patton, C. Zanchetta, R. Fernandes, G. Guella, A. Kale and A. Miotello, Pd-C powder and thin film catalysts for hydrogen production by hydrolysis of sodium borohydride, *Int. J. Hydrogen Energy*, 2008, **33**, 287–292.

11 R. Fiorenza, S. Scirè and A. M. Venezia, Carbon supported bimetallic Ru-Co catalysts for H_2 production through $NaBH_4$ and NH_3BH_3 hydrolysis, *Int. J. Energy Res.*, 2017, **42**, 1183–1195.

12 O. V. Komova, V. I. Simagina, O. V. Netskina, D. G. Kellerman, A. V. Ishchenko and N. A. Rudina, $LiCoO_2$-based catalysts for generation of hydrogen gas from sodium borohydride solutions, *Catal. Today*, 2008, **138**, 260–265.

13 Y. Mu, R. Ma, S. Xue, H. Shang, W. Lu and L. Jiao, Recent advances and perspective on transition metal heterogeneous catalysts for efficient electrochemical water splitting, *Carbon Neutralization*, 2024, **3**, 4–31.

14 L. Chen, B. Lu, J. Zhang, R. Wu and Y. Guo, Integrating trace ruthenium cluster with cobalt boride toward superior overall water splitting in neutral media, *J. Colloid Interface Sci.*, 2022, **623**, 897–904.

15 H. Wang, Nanostructure@metal-organic frameworks (MOFs) for catalytic carbon dioxide (CO_2) conversion in photocatalysis, electrocatalysis, and thermal catalysis, *Nano Res.*, 2021, **15**, 2834–2854.

16 D. Zang, X. J. Gao, L. Li, Y. Wei and H. Wang, Confined interface engineering of self-supported Cu@N-doped graphene for electrocatalytic CO_2 reduction with enhanced selectivity towards ethanol, *Nano Res.*, 2022, **15**, 8872–8879.

17 N. Tsumori, L. Chen, Q. Wang, Q.-L. Zhu, M. Kitta and Q. Xu, Quasi-MOF: exposing inorganic nodes to guest metal nanoparticles for drastically enhanced catalytic activity, *Chem*, 2018, **4**, 845–856.

18 Y. Li, T. Chen, S. Zhao, P. Wu, Y. Chong, A. Li, Y. Zhao, G. Chen, X. Jin, Y. Qiu and D. Ye, Engineering cobalt oxide with coexisting cobalt defects and oxygen vacancies for enhanced catalytic oxidation of toluene, *ACS Catal.*, 2022, **12**, 4906–4917.

19 S. Zhou, Q. Yang, Y. Liu, L. Cheng, T. Taylor Isimjan, J. Tian and X. Yang, Electronic metal-support interactions for defect-induced Ru/Co-Sm_2O_3 mesosphere to achieve efficient $NaBH_4$ hydrolysis activity, *J. Catal.*, 2024, **433**, 115491.

20 L. Wang, J. Huang, Z. Huang, H. Li, T. Taylor Isimjan and X. Yang, Revealing dynamic structural evolution of V and P co-doping-induced Co defects as large-current water oxidation catalyst, *Chem. Eng. J.*, 2023, **472**, 144924.

21 S. Zhou, Y. Yang, W. Zhang, X. Rao, P. Yan, T. T. Isimjan and X. Yang, Structure-regulated Ru particles decorated P-vacancy-rich CoP as a highly active and durable catalyst for $NaBH_4$ hydrolysis, *J. Colloid Interface Sci.*, 2021, **591**, 221–228.

22 L. Shi, K. Zhu, Y. Yang, Y. Liu, S. Xu, T. T. Isimjan and X. Yang, Oxygen-vacancy-rich Ru-clusters decorated Co/Ce oxides modifying ZIF-67 nanocubes as a high-efficient catalyst for $NaBH_4$ hydrolysis, *Int. J. Hydrogen Energy*, 2022, **47**, 37840–37849.

23 Z. Tian, K. Zhou, M. Xie, Y. Zhang, J. Chen, C. Du and L. Wan, Self-supported nickel iron selenide@nickel cobalt boride core-shell nanosheets electrode for asymmetric supercapacitors, *Chem. Eng. J.*, 2022, **447**, 137495.

24 T. Kavinkumar, S. Seenivasan, H. Jung, J. W. Han and D.-H. Kim, Atomic layer deposition-triggered hierarchical core/shell stable bifunctional electrocatalysts for overall water splitting, *J. Mater. Chem. A*, 2021, **9**, 21132–21141.

25 Y. Liu, H. Zhang, W. Song, Y. Zhang, Z. Hou, G. Zhou, Z. Zhang and J. Liu, In-situ growth of ReS_2/NiS heterostructure on Ni foam as an ultra-stable electrocatalyst for alkaline hydrogen generation, *Chem. Eng. J.*, 2023, **451**, 138905.

26 Y. Zhang, P. Chen, Q. Wang, Q. Wang, K. Zhu, K. Ye, G. Wang, D. Cao, J. Yan and Q. Zhang, High-capacity and kinetically accelerated lithium storage in MoO_3 enabled by oxygen vacancies and heterostructure, *Adv. Energy Mater.*, 2021, **11**, 2101712.

27 Y. Guo, B. Chang, T. Wen, S. Zhang, M. Zeng, N. Hu, Y. Su, Z. Yang and B. Yang, A Z-scheme photocatalyst for enhanced photocatalytic H_2 evolution, constructed by growth of 2D plasmonic MoO_{3-x} nanoplates onto 2D g-C_3N_4 nanosheets, *J. Colloid Interface Sci.*, 2020, **567**, 213–223.

28 F. Haque, A. Zavabeti, B. Y. Zhang, R. S. Datta, Y. Yin, Z. Yi, Y. Wang, N. Mahmood, N. Pillai, N. Syed, H. Khan, A. Jannat, N. Wang, N. Medhekar, K. Kalantar-zadeh and J. Z. Ou, Ordered intracrystalline pores in planar molybdenum oxide for enhanced alkaline hydrogen evolution, *J. Mater. Chem. A*, 2019, **7**, 257–268.

29 D. Guo, L. Wen, T. Wang and X. Li, Electrodeposition synthesis of cobalt-molybdenum bimetallic phosphide on nickel foam for efficient water splitting, *J. Colloid Interface Sci.*, 2024, **659**, 707–717.

30 B. Zhao, W. Zeng, W. Zhang, S. Chen, H. Xu, Y. Liao, Y. Liao, Y. Qing and Y. Wu, Tailored bimetallic synergy of iron-cobalt sulfide anchored to S-doped carbonized wood fiber for high-efficiency oxygen evolution reaction, *Appl. Catal., B*, 2024, **350**, 123947.

31 Z. Haiyang, L. Jie, L. Zhiqiang, S. Yayun, Z. Siyan, W. Junchuan, S. Ying, Z. Xueqin and L. Baoping, Influence of Co-MOF morphological modulation on its electrochemical performance, *J. Phys. Chem. Solids*, 2022, **160**, 110336.

32 P. Bhavani, S. Kamalakannan, D. P. Kumar, H. C. Ham, Y.-K. Park and W. Kim, Preferential heteroatom substitution into $ZnIn_2S_4$ nanosheets boosts photocatalytic hydrogen production, *Appl. Catal., B*, 2024, **356**, 124154.

33 Y. He, Y. Yang, C. R. Bowen, Z. Shu, L. Zheng, N. Tu, T. Lu, W. Li and W. Yang, Double-plasmonic-coupled heterojunction photocatalysts for highly-efficient full-spectrum-light-driven H_2 evolution from ammonia borane, *Chem. Eng. J.*, 2024, **481**, 148299.

34 X. Chen, Z. Zhang, S. Zhou, Y. Wei, S. Han and J. Jiang, In-situ growth transformation and oxygen vacancy synergistic modulation of the electronic structure of NiCo-LDH

enables high-performance hybrid supercapacitors, *Appl. Energy*, 2024, **371**, 123670.

35 S. Jiang, R. Zhang, H. Liu, Y. Rao, Y. Yu, S. Chen, Q. Yue, Y. Zhang and Y. Kang, Promoting formation of oxygen vacancies in two-dimensional cobalt-doped ceria nanosheets for efficient hydrogen evolution, *J. Am. Chem. Soc.*, 2020, **142**, 6461–6466.

36 M. Sathiya, J. B. Leriche, E. Salager, D. Gourier, J. M. Tarascon and H. Vezin, Electron paramagnetic resonance imaging for real-time monitoring of Li-ion batteries, *Nat. Commun.*, 2015, **6**, 6276.

37 Y. Luo, Y. Xia, H. Zhou, C. Yin, H. Yang, J. Chen and L. Ou, Effect of calcium ions on surface properties of chalcopyrite and arsenopyrite and its response to flotation separation under low-alkalinity conditions, *Appl. Surf. Sci.*, 2022, **602**, 154191.

38 Z. Chen, R. Zheng, H. Zou, R. Wang, C. Huang, W. Dai, W. Wei, L. Duan, B.-J. Ni and H. Chen, Amorphous iron-doped nickel boride with facilitated structural reconstruction and dual active sites for efficient urea electrooxidation, *Chem. Eng. J.*, 2023, **465**, 142684.

39 Y. Wu, Y. Chen, D. Li, D. Sajjad, Y. Chen, Y. Sun, S. Liu, J. Shi and Z. Jiang, Interface engineering of organic-inorganic heterojunctions with enhanced charge transfer, *Appl. Catal., B*, 2022, **309**, 121261.

40 M. Ma, G. Li, W. Yan, Z. Wu, Z. Zheng, X. Zhang, Q. Wang, G. Du, D. Liu, Z. Xie, Q. Kuang and L. Zheng, Single-atom molybdenum engineered platinum nanocatalyst for boosted alkaline hydrogen oxidation, *Adv. Energy Mater.*, 2022, **12**, 2103336.

41 G. G. Eshetu, T. Diemant, M. Hekmatfar, S. Grugeon, R. J. Behm, S. Laruelle, M. Armand and S. Passerini, Impact of the electrolyte salt anion on the solid electrolyte interphase formation in sodium ion batteries, *Nano Energy*, 2019, **55**, 327–340.

42 S. Chowdhury, N. L. Torad, A. Ashok, G. Gumilar, W. Chaikittisilp, R. Xin, P. Cheng, M. I. Ul Hoque, M. A. Wahab, M. R. Karim, B. Yuliarto, M. S. Hossain, Y. Yamauchi and Y. V. Kaneti, Template-and etching-free fabrication of two-dimensional hollow bimetallic metal-organic framework hexagonal nanoplates for ammonia sensing, *Chem. Eng. J.*, 2022, **450**, 138065.

43 G. Peng, J.-W. Zhao, J. Wang, E. Hoenig, S. Wu, M. Wang, M. He, L. Zhang, J.-X. Liu and C. Liu, Crystal structures of molybdenum borides dictate electrocatalytic ammonia synthesis efficiency, *Appl. Catal., B*, 2023, **338**, 123020.

44 M. S. A. Sher Shah, V. K. Paidi, H. Jung, S. Kim, G. Lee, J. W. Han, K.-S. Lee and J. H. Park, Unprecedented electrocatalytic oxygen evolution performances by cobalt-incorporated molybdenum carbide microflowers with controlled charge re-distribution, *J. Mater. Chem. A*, 2021, **9**, 1770–1783.

45 W. Zhang, L. Yang, Z. Li, G. Nie, X. Cao, Z. Fang, X. Wang, S. Ramakrishna, Y. Long and L. Jiao, Regulating hydrogen/oxygen species adsorption via built-in electric field-driven electron transfer behavior at the heterointerface for efficient water splitting, *Angew. Chem., Int. Ed.*, 2024, **63**, e202400888.

46 D.-W. Zhuang, Q. Kang, S. S. Muir, X. Yao, H.-B. Dai, G.-L. Ma and P. Wang, Evaluation of a cobalt-molybdenum-boron catalyst for hydrogen generation of alkaline sodium borohydride solution-aluminum powder system, *J. Power Sources*, 2013, **224**, 304–311.

47 Y.-S. Feng, Y.-N. Li, P. Wang, Z.-P. Guo, F.-F. Cao and H. Ye, Work-function-induced interfacial electron/ion transport in carbon hosts toward dendrite-free lithium metal anodes, *Angew. Chem., Int. Ed.*, 2023, **62**, e202310132.

48 Y. Song, M. Sun, S. Zhang, X. Zhang, P. Yi, J. Liu, B. Huang, M. Huang and L. Zhang, Alleviating the work function of vein-Like Co_xP by Cr doping for enhanced seawater electrolysis, *Adv. Funct. Mater.*, 2023, **33**, 2214081.

49 V. G. Deonikar, A. Rajkamal and H. Kim, 3D hollow microrod engineered MOF-derived Cu/Co catalysts promoted by Al nanoflakes for efficient H_2 generation through $NaBH_4$ hydrolysis: Perceptions on boosted reaction channels aided by a synergistic effect, *Sustainable Mater. Technol.*, 2023, **38**, e00711.

50 Y. Li, J. Liao, Y. Feng, J. Li, Q. Liu, W. Zhou, M. He and H. Li, Built-in electric field in yolk shell CuO-Co_3O_4@Co_3O_4 with modulated interfacial charge to facilitate hydrogen production from ammonia borane methanolysis under visible light, *Adv. Funct. Mater.*, 2024, 2405361, DOI: **10.1002/adfm.202405361**.

51 S. Zhou, L. Cheng, Y. Huang, Y. Liu, L. Shi, T. T. Isimjan and X. Yang, Constructing Ru particles decorated Co_3B-CoP heterostructures as a highly active and reusable catalyst for H_2 generation by catalyzing $NaBH_4$ hydrolysis, *Appl. Catal., B*, 2023, **328**, 122519.

52 J. Kirk, Y. Kim, Y.-J. Lee, M. Kim, D.-S. Min, P. Soon Kim, J. Hui Seo, Y. Kim, J. Lee, J. Woo Choung, H. Sohn, S.-W. Nam, C.-W. Yoon, Y. Kim and H. Jeong, Pushing the limits of sodium borohydride hydrolysis for on-board hydrogen generation systems, *Chem. Eng. J.*, 2023, **466**, 143233.

53 U. B. Demirci and P. Miele, Reaction mechanisms of the hydrolysis of sodium borohydride: A discussion focusing on cobalt-based catalysts, *C. R. Chim.*, 2014, **17**, 707–716.

54 H. Gu, J. Lan, Y. Liu, C. Ling, K. Wei, G. Zhan, F. Guo, F. Jia, Z. Ai, L. Zhang and X. Liu, Water enables lattice oxygen activation of transition metal oxides for volatile organic compound oxidation, *ACS Catal.*, 2022, **12**, 11272–11280.

55 H. Li, X. Hu, L. Wang, L. Shi, T. T. Isimjan and X. Yang, Kinetically promoted hydrogen generation by Ru nanoparticles decorated CoB_2O_4 on mesoporous carbon spheres with rich oxygen vacancies for $NaBH_4$ hydrolysis, *Chem. Eng. J.*, 2024, **481**, 148547.

56 X. Liu, X. Jin, J. Yan, S. Fan, Y. Wang and D. Astruc, "On-off" control for on-demand H_2 evolution upon Si-H bond hydrolysis: A combined experimental and theoretical study, *Appl. Catal., B*, 2023, **324**, 122261.